RSC Advances

PAPER

View Article Online
View Journal | View Issue



Cite this: *RSC Adv.*, 2017, **7**, 37852

# First principles DFT study of interstitial hydrogen and oxygen atoms in the MAX phase $Ti_2AlN$

Francesco Colonna [ab] and Christian Elsässer [ba]

Received 4th May 2017
Accepted 19th July 2017

DOI: 10.1039/c7ra05045c

rsc.li/rsc-advances

MAX phases are ternary metal carbides and nitrides with multi-layered crystal structures and mixed metallic-covalent bonding. They have very good thermal, chemical, and mechanical properties which make them potentially suitable as corrosion protection coatings for high-temperature energy-conversion devices such as solid oxide fuel cells. To assess the capability of MAX phases as diffusion barriers for hydrogen and oxygen, we investigate absorption and migration of interstitial H and O atoms in the MAX phase $Ti_2AlN$ by means of first-principles calculations based on density functional theory. The resulting calculated formation and migration energies indicate that a $Ti_2AlN$ coating can act as a protective diffusion barrier for both oxygen and hydrogen, but according to two different mechanisms.



## 1 Introduction

MAX phases are a class of ternary nano-multi-layered crystalline compounds which exhibit an outstanding combination of high mechanical stiffness, electrical and thermal conductivity, corrosion resistance, and tolerance to thermomechanical shocks.[1,2] All these properties make MAX phases an interesting class of materials for a wide spectrum of technological applications.

Recently, the proposed applicability of MAX as protective surface coatings of irradiated bulk metallic materials in nuclear fission or fusion reactors has stimulated several simulation studies of properties of atomic defects in MAX phases.[3–5] The investigation of atomic defects, namely their formation and migration properties, is of great interest also for corrosion-protection applications in other thermo-chemo-mechanically aggressive environments. Solid Oxide Fuel Cells (SOFCs) operated at intermediate temperatures are an interesting case for the potential use of MAX phases as protective coatings. The SOFC technology offers an environment-friendly and cost-effective way of efficient energy conversion. However, the success of SOFC stack devices is impeded by the fast corrosive degradation of the stainless-steel interconnect plates between the individual oxydic cells and the concomitant cathode poisoning of the cells.[6,7] Indeed, to prevent the degradation in oxidizing and reducing environments at the operating temperatures of 600–800 °C, interconnect plates made of chromium-alloyed steel[6–8] are used. This material, in turn, is prone to the formation of chromium hydroxides at the surface of the interconnect plate, their subsequent evaporation, and their deposition on the surface of the oxydic cell cathode.

This chromium-poisoning mechanism is often responsible for a rapid decrease in the efficiency of energy conversion in SOFCs.[7–10] Since MAX phases are known to be electrically conducting and stable in both hot and corrosive environments, they offer a good potential to be deployed as a protective surface coating for the steel interconnect plates in SOFCs stacks, and they may also enable the use of steels containing a lower concentration of chromium and thus leading to chromium poisoning at a reduced rate. In order to achieve the goal of long-term stable and efficient SOFC stack devices, it is essential to evaluate the capability of MAX phases as a protective barrier against the diffusion of both hydrogen and oxygen atoms.

Important pre-requisites for MAX phases to be usable in SOFC applications are a good thermal stability at the operation temperature and a coefficient of thermal expansion (CTE) close to those of the ceramic oxide cathodes and electrolytes, which typically range between 10.5 and 12.5 $\times 10^{-6}$ $K^{-1}$.[7,8]

In this work, employing a computational first-principles method based on density functional theory (DFT), we investigate the solution of interstitial hydrogen and oxygen atoms and the pathways and barriers for their migration in the crystal structure of the prominent MAX phase $Ti_2AlN$. The elucidation of the migration mechanisms for interstitial atoms in $Ti_2AlN$ allows to assess the potential of such a MAX phase as a protective coating material. In Section 2 we describe the computational DFT method and the atomistic structure models used for the investigation. In Section 3.1 we report our results on the solution of interstitial H and O atoms in $Ti_2AlN$. In Section 3.2 we illustrate the migration paths, report the calculated energy barriers, and describe the distinct migration mechanisms for H and O. In Section 4 we discuss the results. Finally in Section 5 we make a summary and give some conclusions.

[a]*University of Freiburg, Freiburg Materials Research Center (FMF), Stefan-Meier-Straße 21, 79108 Freiburg, Germany. E-mail: francesco.colonna@fmf.uni-freiburg.de*

[b]*Fraunhofer Institute for Mechanics of Materials IWM, Wöhlerstraße 11, 79108 Freiburg, Germany. E-mail: christian.elsaesser@iwm.fraunhofer.de*

## 2 Structural models and computational method

### 2.1 Composition and structure of the MAX phase $Ti_2AlN$

MAX phases are defined by the composition formula $M_{n+1}A_1X_n$ ($n$ = 1, 2 or 3), where M is a transition-metal element, A is a main-group element, and X is either carbon or nitrogen. Atoms are arranged in a hexagonal crystal structure, space group $P_{63}/mmc$ (193), with $M_{n+1}X_n$ layers interleaved by an A monolayer.

### 2.2 Methodological details of the DFT calculations

To model formation energies and migration barriers of interstitial atoms, a hexagonal $2 \times 2 \times 1$ supercell of the $Ti_2AlN$ crystal was used. The supercell was structurally relaxed by first-principles DFT calculations of total energies, forces, and stresses, using the GGA-PBE functional for exchange–correlation.[11] All DFT calculations were done with the PWscf code of the Quantum Espresso software package[12] and run with an ASE interface.[13] The wave-functions of the valence electrons are represented by a plane-waves basis set with a cutoff energy of 544 eV, and the electron density and effective Kohn–Sham potential by discrete Fourier series with a cutoff energy of 2721 eV. The interactions of valence electrons with the atomic nuclei and core electrons are described by Vanderbilt's ultrasoft pseudopotentials as provided in the open-source pseudopotential library 'GRBV'.[14] Brillouin-zone integrals are evaluated on a Monkhorst–Pack mesh of $6 \times 6 \times 4$ $k$-points with a Gaussian smearing of 0.02 eV. The convergence criteria was set to $1.36 \times 10^{-6}$ eV for the total energy and to $2.57 \times 10^{-4}$ eV Å$^{-1}$ for the forces on atoms.

All thermodynamic quantities were calculated following the *ab initio* thermodynamics formalism[15] at zero pressure and temperature. The solution energy $E^f$[X, i] of an atom X (X = H or O) at an interstitial site i in the supercell of the $Ti_2AlN$ crystal is calculated as

$$E^f[X, i] = E_{tot}[X, i] - E_{tot}[bulk] + \mu_X \quad (1)$$

where $E_{tot}$[X, i] is the total energy of the supercell of the pure crystal with the interstitial atom X, $E_{tot}$[bulk] is the total energy of the reference supercell of the perfect crystal, and $\mu_X$ is the chemical potential of either hydrogen or oxygen. The lattice constants were kept fixed during total energy calculations of point-defects. The chemical potentials with respect to the $H_2$ and $O_2$ gas phases were calculated as half of the binding energies of the $H_2$ and $O_2$ molecules. Our computed values for the binding energies of $H_2$ and $O_2$ are respectively −4.12 eV and −5.93 eV, in line with data from previous calculations.[17] It is known for oxygen that LDA or GGA functionals result in an overbinding with respect the experimental value of −5.22 eV. For a discussion of this issue and possible empirical corrections we refer to, *e.g.*, ref. 17.

To validate the computational methodology, the lattice parameters of $Ti_2AlN$ and formation energies of the three intrinsic point defects, namely the monovacancies $\nu_{Ti}$, $\nu_{Al}$ and $\nu_N$ were calculated and compared to literature benchmarks. Both the resulting lattice-parameter values ($a$ = 2.995 and $c$ = 13.65) and the formation energies for $\nu_{Ti}$, $\nu_{Al}$ and $\nu_N$ (3.48 eV, 3.03 eV, and 4.58 eV respectively) are in agreement with data from previous experimental measurements[18] and DFT simulations.[4] In Fig. 1 we compare our results for the vacancy formation energies (top) and the chemical potentials (bottom) to literature data.

### 2.3 Interstitial sites for H and O atoms in the MAX phase $Ti_2AlN$

Following the work of Baben *et al.*[19] on $Ti_2AlC$, Duan *et al.*[4] investigated the solution of oxygen and hydrogen atoms at substitutional positions as well as at octahedral ($Ti_3Al_3$) and triangular ($Al_3$) interstitial sites of the $Ti_2AlN$ crystal. Cui *et al.*[20] reported that the dynamics of oxidation of $Ti_2AlN$ differs from that of $Ti_2AlC$. Therefore we extended the previous studies by considering the whole set of interstitial locations in the $Ti_2Al$ (Ti–Al–Ti) double layer which are relevant for the solution and migration of H and O atoms (see Fig. 2): the $Ti_3Al_3$ octahedron, the $Ti_3Al$ and $TiAl_3$ tetrahedrons, and the two non-equivalent triangular barrier locations $Al_3^I$ and $Al_3^{II}$ in the Al-plane. Moreover, $Ti_4$ tetrahedral sites in the $Ti_2N$ (Ti–N–Ti) double layer are also considered.

The migration barriers were assumed to be located either at the interface of face-sharing polyhedrons (see Fig. 2), or at the

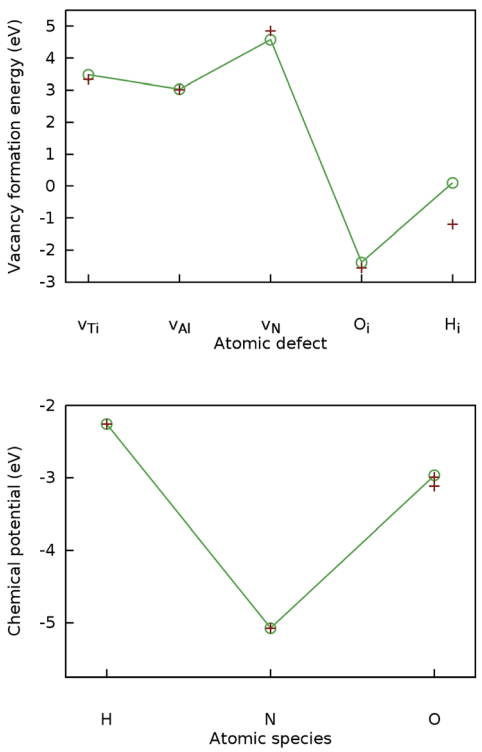


Fig. 1 Validation of the computational DFT setup. Top: Calculated formation energies (connected by lines) for the Ti, Al, and N vacancies in $Ti_2AlN$ and for the H and O interstitials in the octahedral position $Ti_3Al_3$ compared to literature benchmarks[4] (crosses). Bottom: Calculated chemical potentials (connected by lines) for H, N, and O compared to literature benchmarks[16] (crosses).

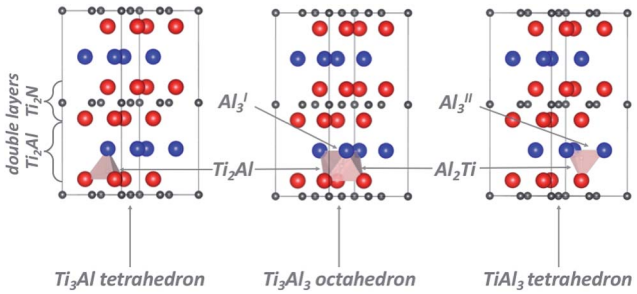


Fig. 2 Schematic representation of the $Ti_2AlN$ supercell. Ti atoms are represented by red spheres, Al by blue ones, and N by grey ones. Polyhedra $Ti_3Al_3$, $Ti_3Al$, and $TiAl_3$ in the $Ti_2Al$ (Ti–Al–Ti) layer are shown explicitly; grey arrows point to the triangular interfaces $Ti_2Al$, $Al_2Ti$, $Al_3^{I}$, and $Al_3^{II}$.

centre of N–N bonds of the $Ti_2Al$ (Ti–Al–Ti) double layer for symmetry considerations. Migration barriers were obtained *via* a structural relaxation in which hydrogen atoms were constrained either on the planes spanned by triangles on the polyhedron's faces, or at the N–N bond centres.

# 3 Results

## 3.1 Solution of interstitial H and O atoms

Baben *et al.* reported that interstitial sites are the most stable sites for atomic species dissolved in $Ti_2AlC$ and other MAX-phase carbides.[19]

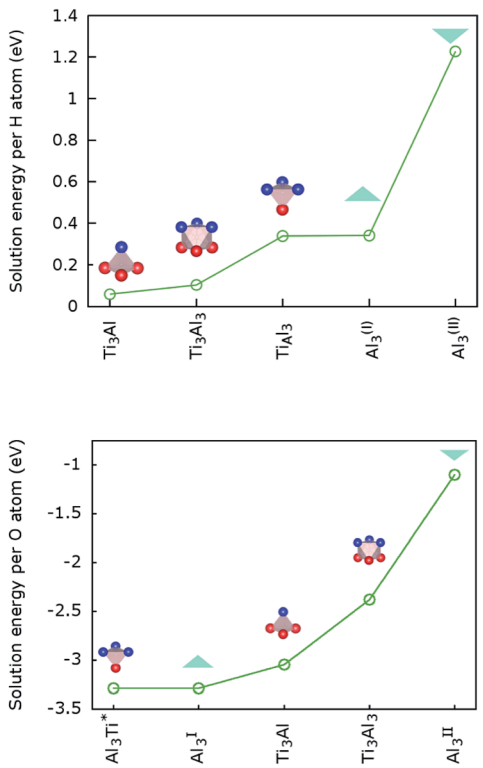


Fig. 3 Solution energies of interstitial hydrogen (top) and oxygen (bottom) in $Ti_2AlN$.

Our results for H atoms in $Ti_2AlN$, which are displayed in Fig. 3 (top), are that hydrogen has a positive (endothermal) solution energy for all the interstitial sites introduced in Section 2.3. This means that H does not dissolve spontaneously in crystalline $Ti_2AlN$. Its most (meta-)stable interstitial site is the tetrahedral site $Ti_3Al$ with an endothermal but close to zero solution energy of 0.06 eV. The octahedral site $Ti_3Al_3$ is the next (meta-)stable site with an endothermal solution energy of 0.1 eV. Zero point energy (ZPE) correction slightly lowers the computed solution energy for H. However, we do not expect ZPE correction to change any of the conclusions.

In contrast, oxygen exhibits a negative (exothermal) solution energy of several eV for all the interstitial sites. The results are displayed in Fig. 3 (bottom). The most stable positions for an O atom are the tetrahedral site $Al_3Ti$ and the triangular barrier location $Al_3$. Their very small energy difference is within the computational accuracy limit. Since the $Al_3$ triangle is the interface separating two mirror-imaged $Al_3Ti$ tetrahedra, these two geometrical locations are effectively within one single site surrounded by a triangular bipyramidal $Al_3Ti_2$ cage. The solution energy for this site is −5.51 eV. The solution energies of the tetrahedral $Ti_3Al$ and octahedral $Ti_3Al_3$ sites are higher by 0.24 and 0.91 eV, respectively. For the interstitial oxygen atom at the $Ti_3Al_3$ site our calculated solution-energy value −2.38 eV is 0.18 eV higher than the value reported by Duan *et al.*[4]

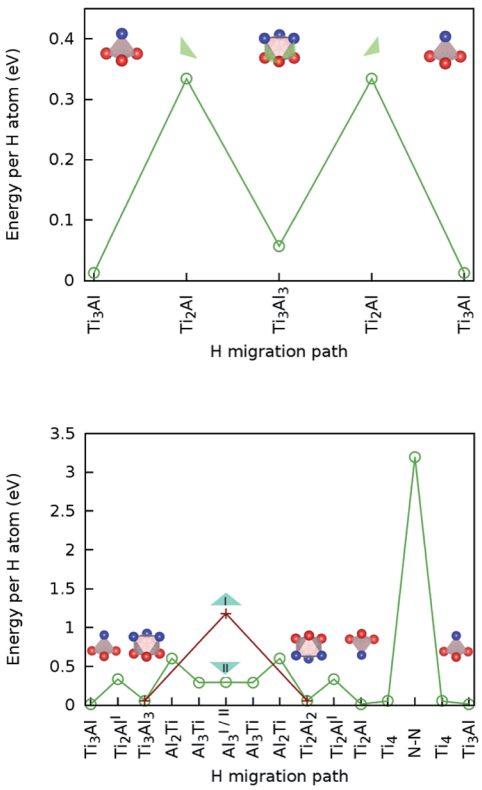


Fig. 4 (Top) Hydrogen lateral migration barriers (*i.e.* in a Ti–Al plane) between tetrahedral stable sites; (bottom) transversal migration barriers (*i.e.* between adjacent Ti–Al planes and through the $Ti_2N$ double layer) between tetrahedral stable sites.

### 3.2 Migration of interstitial H and O atoms

**3.2.1 Hydrogen.** By calculating the migration barriers between interstitial sites, the energetically most favourable migration paths were identified (Fig. 4). The migration barrier between polyhedral sites is assumed to be located on or at least very close to their shared face. The $Ti_3Al_3$ octahedra are connected to $Ti_3Al$ and $TiA_3l$ tetrahedra through $Ti_2Al$ and $TiAl_2$ faces, respectively, as shown in Fig. 2. The $Ti_3Al_3$ octahedra and $Ti_3Al$ tetrahedra are connected to mirror-images with respect to the plane of Al atoms by the triangles labelled $Al_3^{I}$ and $Al_3^{II}$. Finally, the transition state for the migration of an interstitial atom through a $Ti_2N$ double layer is assumed to be centred at a N–N bond. The reason for this choice is the following: the octahedral sites $Al_3Ti_3$ in the $Ti_2N$ double layer are occupied by nitrogen atoms, while the tetrahedral sites $Ti_3Al$ therein are free to host interstitial atoms. To migrate through the $Ti_2N$ double layer, a hydrogen or oxygen atom needs therefore first to enter a $Ti_3Al$ tetrahedron and next to migrate to a mirror-imaged one by crossing an edge of $Al_3Ti_3$ at the mid point of the edge, *i.e.* at the centre of a N–N bond.

The calculated lowest migration-barrier value for interstitial hydrogen resulted to be 0.32 eV for the path $TiAl_3 \rightarrow Ti_3Al_3$. The inverse path has a slightly lower barrier of 0.28 eV. The barrier for the path $Ti_3Al_3 \rightarrow Ti_3Al$ is about twice as high. These results indicate the presence of two parallel, mirror-imaged, diffusion networks in between neighbouring Ti and Al layers, as illustrated in Fig. 5 (right). Indeed, a hydrogen atom can get to the mirror-imaged Ti–Al layer *via* the path $Ti_3Al \rightarrow Ti_3Al_3 \rightarrow TiAl_3 \rightarrow Ti_3Al_3 \rightarrow Ti_3Al_3^{mirror} \rightarrow Ti_3Al^{mirror}$. This migration path has a barrier of 1.2 eV, which is associated with the $Ti_3Al_3 \rightarrow TiAl_3$ step and located in the $Al_3^{I}$ triangle. A schematic representation of these diffusion channels is shown in Fig. 5 (left). An interstitial H atom migrating in the *c*-axis direction of the MAX crystal, with a transition state assumed in a N–N bond as motivated above, has to overcome a high barrier of more than 3 eV, which is one order of magnitude higher than the barriers in the *ab*-plane directions.

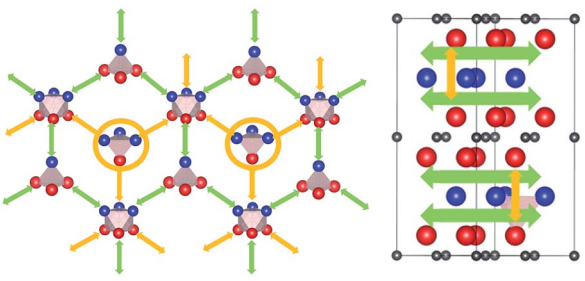

Fig. 5 (Left) Schematic representation of migration paths of interstitial hydrogen in $Ti_2AlN$ highlighting the in-plane migration network in the $Ti_2Al$ double layer. Green arrows indicate the path with the lowest migration barrier between $Ti_3Al$ interstitials. Yellow circles indicate the metastable states from where a migration between mirror-imaged Ti–Al planes is possible. (Right) Hydrogen migration path in the transversal direction. Green arrows indicates the in-plane migration network in the $Ti_2Al$ double layer, while yellow arrows indicates the transition between mirror-imaged Ti–Al planes.

Hence, the network of migration pathways for long-range diffusion of interstitial H atoms in $Ti_2AlN$ can be described as follows: there are two mirror-imaged honey-comb networks between two neighbouring planes of Ti and Al atom with a migration barrier of 0.32 eV. These networks enable the long-range diffusion in the "lateral" directions, *i.e.* in the *ab*-plane spanned by the lattice vectors $\vec{a}$ and $\vec{b}$ of the hexagonal cell. The networks are further connected by a shifted hexagonal network with a barrier of 1.2 eV, which allows for a migration in the *c*-axis (transversal) direction at least between the adjacent $Ti_2Al$ double layer. The migration to a more remote $Ti_2Al$ double layer is hindered by the presence of the $Ti_2N$ double layer in between, with a barrier that is one order of magnitude higher. This network of pathways is illustrated by the schematic sketches in Fig. 5.

**3.2.2 Oxygen.** The diffusion of interstitial oxygen was investigated on the same network of sites and paths as for interstitial hydrogen. However, as discussed above, in this case the two mirror-imaged tetrahedra $Al_3Ti$ connected by the same $A_3$ interface do effectively form one single interstitial transition state in the center of the trigonal bipyramid $Al_3Ti_2^*$. Therefore in the case of oxygen the channels for long-range diffusion in the two mirror-imaged planes of the $Ti_2Al$ double layer are separated by virtually no barrier. As a result, there is one single effective honey-comb network for the *ab*-plane diffusion that connects directly two stable interstitial sites along the migration path $Al_3Ti_2^* \rightarrow Al_3Ti_3 \rightarrow Al_3Ti_2^*$.

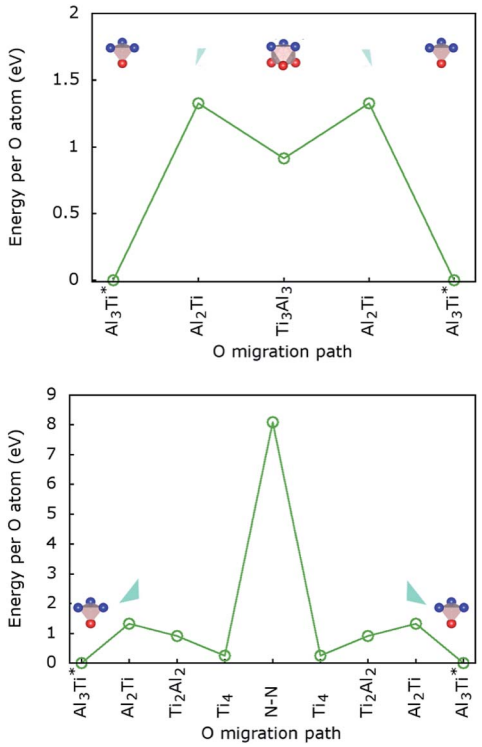


Fig. 6 (Top) Oxygen lateral migration barriers (*i.e.* in a Ti–Al plane) between tetrahedral stable sites; (bottom) oxygen transversal migration barriers (*i.e.* between adjacent Ti–Al planes and through the $Ti_2N$ double layer) between tetrahedral stable sites.

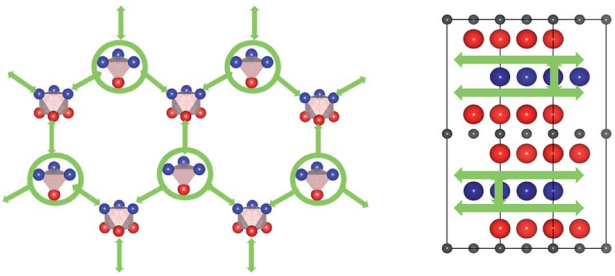

Fig. 7 Schematic representation of interstitial diffusion paths of oxygen in $Ti_2AlN$. (Left) In-plane migration network in the $Ti_2Al$ double layer. Circles indicate the stable $Al_3Ti_2^*$ interstitial connecting the two mirror-imaged TiAl planes. (Right) Oxygen migration path in the transversal direction.

The migration barrier for the path $Al_3Ti_2^* \rightarrow Al_3Ti_3$ is 1.37 eV and located at the triangular $Al_2Ti$ face as shown in Fig. 6. The barrier for the inverse path $Al_3Ti_3 \rightarrow Al_3Ti_2^*$ is 0.42 eV. The interstitial diffusion through the $Ti_2N$ double layers is hindered by a large barrier of over 8 eV (Fig. 6). The resulting diffusion network is depicted schematically in Fig. 7. As in the case of hydrogen the *ab*-plane migration for oxygen has a much lower barrier than the *c*-axis migration. In contrast to hydrogen, the *ab*-plane migration of oxygen has a simpler mechanism, namely $Al_3Ti^* \rightarrow Al_3Ti_3 \rightarrow Al_3Ti^*$, on a honey-comb network. But for oxygen there is a more than four times higher barrier as compared to that of hydrogen.

## 4 Discussion

There is only few discussion in literature about the absorption and diffusion of hydrogen in MAX phases. A MAX phases coating can protect a substrate from diffusing hydrogen in two ways: (1) by a high migration barrier, and (2) by a high solution energy, which hinders the absorption of the diffusing species in a first place. In the literature hydrogen absorption on interstitial sites is reported to be favoured by a slightly negative (exothermal) energy of solution, however depending on its chemical potential as function of the thermodynamic conditions.[4] In the hydrogen-rich limit, instead, we get a close-to-zero but positive (endothermal) solution energy of 0.06 eV for a H atom at a $Al_3Ti$ site. This value is lower than the solution energy of hydrogen in α-iron (DFT-GGA values: 0.19 eV,[21] 0.16;[22] experimental values: 0.296 eV,[23] 0.28 eV [24]), which indicates that $Ti_2AlN$ cannot act as a diffusion barrier for iron-based interconnects by hindering absorption.

The calculated migration barriers for both interstitial H and O atoms indicate strongly anisotropic diffusion in the MAX phase. Even in the absence of other atomic or microstructural defects, hydrogen is expected to be relatively mobile along the Ti–Al *ab*-planes because of its modest activation barrier of 0.32 eV for migration. This value can be compared to the *ab*-plane diffusion in the MAX phase $Ti_3AlC_2$, which was recently calculated by Yang *et al.*[25] Here two non-equivalent barriers of 0.21 eV and 0.67 eV along the [−1, 0, 0] and [0, 1, 0] directions were found, indicating as well a fast *ab*-plane diffusion of interstitial hydrogen. Hence, the potential of $Ti_2AlN$ as a diffusion barrier for hydrogen is apparently linked to the capability of depositing dense $Ti_2AlN$ films with the *ab*-plane atomic layers of Ti, Al, and N growing parallel to the surface of the substrate. In this case the high migration barrier of the $Ti_2N$ double layer in the *c*-axis direction can effectively impede the diffusion of hydrogen.

The situation is more complicated for the case of oxygen. Recently Cui *et al.*[20] investigated spark plasma sintered $Ti_2AlN$ and its oxydic surface scales formed after high-temperature oxidation for 1 hour. Below 900 °C (*i.e.* at operation temperatures of SOFCs) a double-layer scale is formed: the first layer is composed of porous $TiO_2$ scale in contact with the bulk $Ti_2AlN$ phase, the second layer is a dense mixture of $TiO_2$ and α-$Al_2O_3$ with a nominal composition $Al_2TiO_5$. At higher temperatures (1000–1400 °C), a complex interplay of mixing and demixing of α-$Al_2O_3$ and $Al_2TiO_5$ phases is observed. Above 1100 °C the growth rate of the scale increases steeply and void-containing layers are formed, probably due to the formation of gaseous $NO_x$. These temperatures are above the stability limit of the MAX phase, as reported by Scabarozi *et al.*[26] The emerged scenario is consistent with our finding that oxygen tends to be absorbed interstitially in $Ti_2Al$ double layers and to diffuse along these. Only at very high temperatures there may be some incorporation of oxygen atoms into the $Ti_2N$ double layers, which may be also facilitated by dislocations or cracks induced by the mismatch in the thermal expansions of the oxydic constituents of the scale and the bulk MAX phase. It is not clear whether complicated mixing and demixing of $TiO_2$, α-$Al_2O_3$, and $Al_2TiO_5$ should be expected for longer operation times of SOFCs also at temperatures below 900 °C. Zhang *et al.*[27] showed that thin films of $Ti_2AlN$ oxidized at 900 °C for 20 hours have an α-$Al_2O_3$ scale with a low content of $TiO_2$ second phase growing parabolically in time. This indicates a diffusion-limited growth mechanism, which can be associated to slow diffusion of oxygen through the surface scale and into the $Ti_2AlN$. Moreover, they find a low oxygen content in the interior of the $Ti_2AlN$ layer, which also indicates a diffusion rate which is significantly lower than that of H atoms, in line with our results. The analysis of results of simulations and experiments, therefore, indicates that for the case of oxygen a two-fold protection mechanism is apparently present. First, due to the formation of an oxydic scale, solution of oxygen inside the MAX phase is hindered, except for an adsorption on the surface. Second, due to a high migration barrier for interstitial oxygen in all crystal directions of the MAX phase, the oxydic scale remains confined to the surface. In contrast to the case of hydrogen, the migration barrier for oxygen is therefore expected to be significantly high even for the diffusion in the *ab*-plane of the MAX-phase crystal.

## 5 Summary and conclusions

Solution and migration of interstitial hydrogen and oxygen atoms in the MAX-phase crystal $Ti_2AlN$ were investigated in order to assess the potential capability of a MAX phase to act as a protective diffusion-barrier coating of steel components in SOFC stacks. There are further mechanisms for the solution

 

and migration of hydrogen and oxygen relevant in practice, namely substitutional solution and vacancy-mediated diffusion of foreign atomic species inside the crystal structure or at extended microstructural defects, namely dislocations and grain boundaries. The present study, however, focused on the evaluation of the protection potential of $Ti_2AlN$ by assessing the case of the ideal crystalline limit, where no other defects than the interstitial H or O atoms are present. We obtained solution energies and migration barriers by means of first-principles DFT calculations. The results indicate that a $Ti_2AlN$ coating layer can act as a barrier against diffusion of interstitial H atoms in the *c*-axis direction of the MAX phase but offers no significant protection against diffusion along *ab*-plane directions. For interstitial O atoms, in contrast, the migration barriers in all directions are of the order of several eV. Moreover, absorption calculations and experimental results reported in the literature suggest that, when the surface of a MAX phase is in contact with oxygen, alumina and titania scales are formed. Hence, we speculate that a $Ti_2AlN$ coating on a steel interconnect plate has the potential to act as a protective diffusion barrier for hydrogen and oxygen in a SOFC stack, provided that the formation of a compact, coarse-grained, well *c*-axis oriented, and well *ab*-plane textured $Ti_2AlN$ coating can be achieved on steel by a robust and efficient deposition process.

## Acknowledgements

This research is supported by the Baden-Württemberg Stiftung GmbH through the research programme "CleanTech" (project CT-6 "LamiMat"). We thank Dr D. Di Stefano, Mr L. Gröner, and Dr F. Burmeister for valuable discussions, and Dr B. Ziebarth for his interface of the PWScf code to the ASE software.

## References

1 M. W. Barsoum, *Prog. Solid State Chem.*, 2000, **28**, 201–281.
2 P. Eklund, M. Beckers, U. Jansson, H. Högberg and L. Hultman, *Thin Solid Films*, 2010, **518**, 1851–1878.
3 S. C. Middleburgh, G. R. Lumpkin and D. Riley, *J. Am. Ceram. Soc.*, 2013, **96**, 3196–3201.
4 J. Z. Duan, J. R. Zhang, C. L. Wang, Y. Qiu, W. S. Duan and L. Yang, *RSC Adv.*, 2014, **4**, 42014–42021.
5 Z. Zhang, H. Jin, J. Pan, J. Chai, L. M. Wong, M. B. Sullivan and S. J. Wang, *J. Phys. Chem. C*, 2015, **119**, 16606–16613.
6 J. Wu and X. Liu, *J. Mater. Sci. Technol.*, 2010, **26**, 293–305.
7 N. Mahato, A. Banerjee, A. Gupta, S. Omar and K. Balani, *Prog. Mater. Sci.*, 2015, **72**, 141–337.
8 G. Jia and L. Yang, *Phys. B*, 2010, **405**, 4561–4564.
9 J. Fergus, *Int. J. Hydrogen Energy*, 2007, **32**, 3664–3671.
10 N. Shaigan, W. Qu, D. G. Ivey and W. Chen, *J. Power Sources*, 2010, **195**, 1529–1542.
11 J. P. Perdew, K. Burke and M. Ernzerhof, *Phys. Rev. Lett.*, 1996, **77**, 3865–3868.
12 P. Giannozzi, S. Baroni, N. Bonini, M. Calandra, R. Car, C. Cavazzoni, D. Ceresoli, G. L. Chiarotti, M. Cococcioni, I. Dabo, A. Dal Corso, S. de Gironcoli, S. Fabris, G. Fratesi, R. Gebauer, U. Gerstmann, C. Gougoussis, A. Kokalj, M. Lazzeri, L. Martin-Samos, N. Marzari, F. Mauri, R. Mazzarello, S. Paolini, A. Pasquarello, L. Paulatto, C. Sbraccia, S. Scandolo, G. Sclauzero, A. P. Seitsonen, A. Smogunov, P. Umari and R. M. Wentzcovitch, *J. Phys.: Condens. Matter*, 2009, **21**, 395502.
13 S. R. Bahn and K. W. Jacobsen, *Comput. Sci. Eng.*, 2002, **4**, 56–66.
14 K. F. Garrity, J. W. Bennett, K. M. Rabe and D. Vanderbilt, *Comput. Mater. Sci.*, 2014, **81**, 446–452.
15 C. G. V. de Walle and J. Neugebauer, *J. Appl. Phys.*, 2004, **95**, 3851–3879.
16 C. Freysoldt, B. Grabowski, T. Hickel, J. Neugebauer, G. Kresse, A. Janotti and C. G. Van de Walle, *Rev. Mod. Phys.*, 2014, **86**, 253–305.
17 L. Wang, T. Maxisch and G. Ceder, *Phys. Rev. B: Condens. Matter Mater. Phys.*, 2006, **73**, 5419–5423.
18 M. W. Barsoum, M. Ali and T. El-Raghy, *Metall. Mater. Trans. A*, 2000, **31**, 1857–1865.
19 M. Baben, L. Shang, J. Emmerlich and J. M. Schneider, *Acta Mater.*, 2012, **60**, 4810–4818.
20 B. Cui, D. D. Jayaseelan and W. E. Lee, *Acta Mater.*, 2011, **59**, 4116–4125.
21 D. E. Jiang and E. A. Carter, *Phys. Rev. B: Condens. Matter Mater. Phys.*, 2004, **70**, 064102.
22 D. Di Stefano, R. Nazarov, T. Hickel, J. Neugebauer, M. Mrovec and C. Elsässer, *Phys. Rev. B*, 2016, **93**, 184108.
23 J. P. Hirth, *Metall. Trans. A*, 1980, **11**, 861–890.
24 H. Wipf, *Phys. Scr., T*, 2001, **94**, 43–51.
25 S. Yang, N. Hu, X. Gou, C. Wang, X. Zhu, X. Duan, W. Duan and L. Yang, *RSC Adv.*, 2016, **6**, 59875–59881.
26 T. H. Scabarozi, S. Amini, O. Leaffer, A. Ganguly, S. Gupta, W. Tambussi, S. Clipper, J. E. Spanier, M. W. Barsoum, J. D. Hettinger and S. E. Lofland, *J. Appl. Phys.*, 2009, **105**, 13543.
27 T. Zhang, H.-B. Myoung, D.-W. Shin and K. H. Kim, *J. Ceram. Process. Res.*, 2012, **13**, S149–S153.